NANO LETTERS

pubs.acs.org/NanoLett

Letter

Dual-Action Heteromultivalent Glycopolymers Stringently Block and Arrest Influenza A Virus Infection *In Vitro* and *Ex Vivo*

Badri Parshad,[▽] Marlena N. Schlecht,[▽] Morris Baumgardt, Kai Ludwig, Chuanxiong Nie, Agustina Rimondi, Katja Hönzke, Stefano Angioletti-Uberti, Vinod Khatri, Paul Schneider, Andreas Herrmann, Rainer Haag, Andreas C. Hocke, Thorsten Wolff, and Sumati Bhatia*

Cite This: *Nano Lett.* 2023, 23, 4844−4853

Read Online

ACCESS | Metrics & More | Article Recommendations | Supporting Information

ABSTRACT: Here, we demonstrate the concerted inhibition of different influenza A virus (IAV) strains using a low-molecular-weight dual-action linear polymer. The 6′-sialyllactose and zanamivir conjugates of linear polyglycerol are optimized for simultaneous targeting of hemagglutinin and neuraminidase on the IAV surface. Independent of IAV subtypes, hemagglutination inhibition data suggest better adsorption of the heteromultivalent polymer than homomultivalent analogs onto the virus surface. Cryo-TEM images imply heteromultivalent compound-mediated virus aggregation. The optimized polymeric nanomaterial inhibits >99.9% propagation of various IAV strains 24 h postinfection *in vitro* at low nM concentrations and is up to 10000× more effective than the commercial zanamivir drug. In a human lung *ex vivo* multicyclic infection setup, the heteromultivalent polymer outperforms the commercial drug zanamivir and homomultivalent analogs or their physical mixtures. This study authenticates the translational potential of the dual-action targeting approach using small polymers for broad and high antiviral efficacy.

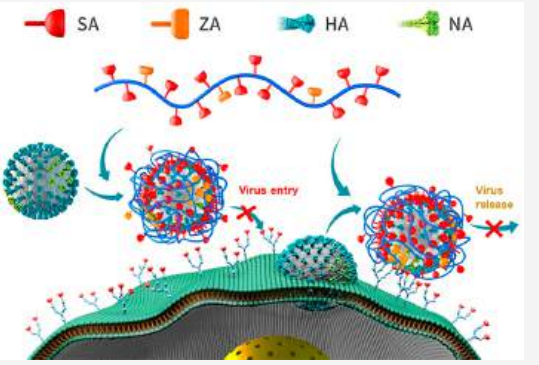

KEYWORDS: *heteromultivalency, influenza A virus, dual-action linear polymer, glycopolymer, multicyclic infection, broad inhibition*

Influenza A viruses (IAVs) regularly challenge public health globally by causing seasonal epidemics and sporadic pandemics.[1] The unpredictable patterns of IAV antigenic drift and shift make the annual adaptation of vaccines challenging, as exemplified by the recent spread of A/H5N1.[2] Additionaly, recent studies have illustrated that IAV coinfection may enhance the severity of concomitant COVID-19.[3−5]

IAV is an enveloped RNA virus with two surface proteins, the homotrimeric hemagglutinin (HA) that binds to sialic acid (SA) on cell surfaces and the tetrameric neuraminidase (NA), which is a sialidase that cleaves sialoside bonds between HA and SA.[6−9] IAV binding to host cell receptors is highly dynamic, and viruses move along the host cell membrane before being internalized.[10] This process is facilitated by the multivalent attachment of multiple noncovalent HA−SA bonds that can be cleaved by NA, resulting in a directional movement.[7,11]

NA allows virions to move through the highly sialylated host mucus layer, which otherwise could inhibit viral entry into the host system.[12] Overall balance in HA receptor-binding and NA receptor-cleaving activity is pivotal for virus replication and transmission. Commercial anti-influenza drugs such as oseltamivir and zanamivir are NA inhibitors that can prevent the cleavage of sialoside bonds with HA proteins, thus allowing them to interfere with the mobility as well as the release of newly formed virions from the host cell and, consequently, the propagation of infection.[13] The emergence of drug resistance in IAV strains can render these drugs ineffective, as suggested by oseltamivir- and zanamivir-resistant IAVs.[14]

Inhibiting the infection at an early step by targeting the HA to prevent cell binding is a promising approach. Multivalent sialoside-based polymers,[15] dendrimers,[16] nanoparticles,[17,18] nanogels,[19,20] and proteins[21] have overcome the low binding affinity (K_d ∼ 2−4 mM)[22] of monovalent SA to HA through a multivalent effect and have shown significant inhibition of IAV binding to the host cells. However, because of the high variability in the structure and amino acid sequence of the HA binding pockets of different influenza strains, broad activity with high efficacy is still elusive for most polysialylated inhibitors.[23,24] Replacing SA with 6′-sialyllactose (SL), which mimics the natural receptor more closely, extended the activity

Received: February 1, 2023
Revised: May 11, 2023
Published: May 23, 2023

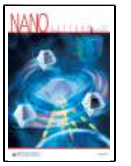

Scheme 1[a]

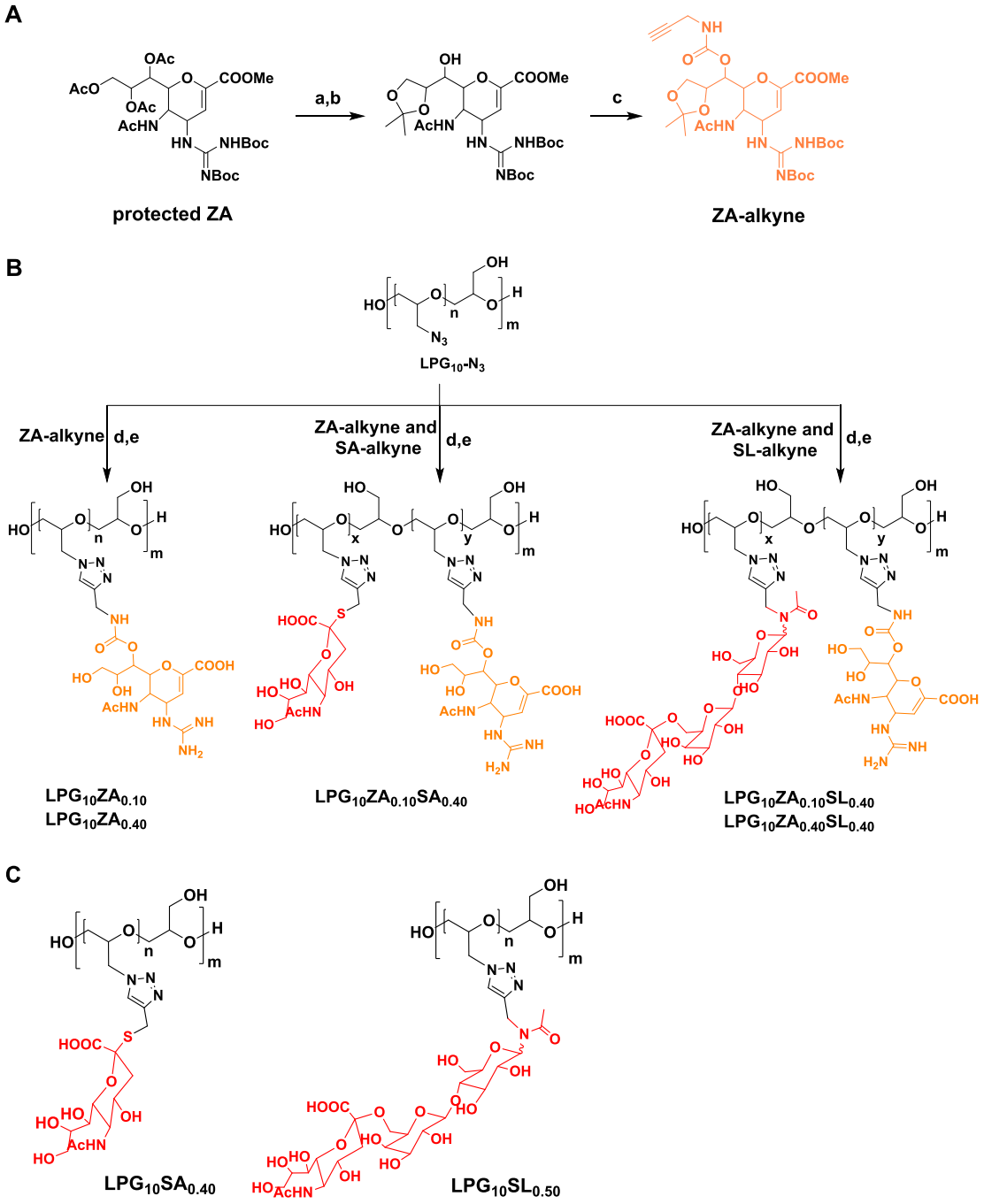

[a](A) Important steps for the synthesis of ZA-alkyne. Reagents and conditions are as follows: (a) NaOMe, MeOH, rt, 4 h; (b) acetone, triflic acid, rt, 4 h; and (c) *p*-nitrophenyl chloroformate, pyridine, DMAP, propargylamine, rt, 16 h. (B) Synthesis of ZA, SA, and SL-functionalized linear polyglycerol polymers. Reagents and conditions are as follows: (d) ZA/SA/SL, $CuSO_4.5H_2O$, sodium ascorbate, DMF/H_2O, 50 °C, 48 h; (e) (i) 2 M aq. NaOH, rt, 5 h and (ii) DCM, TFA, rt, 5 h. (C) Structures of SA- and SL-functionalized linear polyglycerols.

against some IAV strains; high potency has remained a bottleneck.[23]

We have overcome this challenge by developing a heteromultivalent linear polyglycerol (LPG) with zanamivir (ZA) and SL residues, which is highly potent and broadly active against IAV infection. We have chosen 10 kDa LPG for multivalent display because of its excellent water solubility, cytocompatibility, scalability, and good *in vivo* clearance.[24,25] The optimized heteromultivalent presentation of SL and ZA generated a broad activity against different IAV strains. This compound broadly inhibits IAV propagation *in vitro* and in human lung explants at a low nM concentration and is also 3−4 orders of magnitude more potent at inhibiting IAV propagation than the commercially available ZA drug. Our study emphasizes heteromultivalency and suggests synergistic effects against both the binding and release of various IAVs for the first time using a low-molecular-weight biocompatible polymer.

Considering the uniform distribution of 300−500 HA trimers on the IAV surface,[26,27] we have optimized the SA

https://doi.org/10.1021/acs.nanolett.3c00408
Nano Lett. 2023, 23, 4844−4853

Table 1. Characterization of All Compounds Tested against the A/X31 (H3N2) Virus

polymer[a] ($LPG_{10}ZA_{DF}SA_{DF}$)	DF[b] (%)	SA/SL and ZA per polymer[c]	ζ-potential ± SD [mV][d]	NA inhibition IC_{50} ± SD [nM] [ZA][e]
$LPG_{10}OH$			−2.7 ± 1.66	1775 ± 592
$LPG_{10}SA_{0.40}$	SA = 44	SA = 60	−30.8 ± 2.58	1579 ± 336
$LPG_{10}SL_{0.50}$	SL = 50	SL = 67	−18.6 ± 1.72	>10 000
zanamivir				0.97 ± 0.16
$LPG_{10}ZA_{0.10}$	ZA = 10	ZA = 13	−3.3 ± 1.40	2.10 ± 0.41 (27.3)
$LPG_{10}ZA_{0.40}$	ZA = 40	ZA = 54	−17.4 ± 3.48	1.27 ± 0.24 (68.58)
$LPG_{10}ZA_{0.10}SA_{0.40}$	ZA = 13, SA = 40	ZA = 20, SA = 54	−29.5 ± 4.34	0.07 ± 0.01 (1.4)
$LPG_{10}ZA_{0.10}SL_{0.40}$	ZA = 10, SL = 40	ZA = 13, SA = 54	−22.4 ± 3.66	19.58 ± 4.76 (255)
$LPG_{10}ZA_{0.40}SL_{0.40}$	ZA = 40, SL = 40	ZA = 54, SL = 54	−15.9 ± 4.95	4.86 ± 1.25 (262)

[a]Polymer is defined by providing the degree of functionalization (DF) of sialic acid (SA), 6′-sialyllactose (SL), and zanamivir (ZA) residues per hydroxyl group of a 10 kDa LPG polymer. [b]DF is determined by ^{1}HNMR analysis. [c]The number of sialic acid (SA), 6′-sialyllactose (SL), and zanamivir (ZA) units per polymer was calculated using DF values. [d]The ζ-potential was measured in PB (10 mM, 7.4 pH) at a 1 mg/mL concentration. [e]IC_{50} in terms of ZA conjugated with the polymer backbone is given in brackets. Values are obtained using the MUNANA assay with the A/X31 (H3N2) virus. Values are expressed as mean ± SD, $n = 6$.

ligand density on the 10 kDa LPG scaffold as 40−70% for an effective IAV inhibition in our previous reports.[24] Accordingly, SA and SL with 40% and 50% degree of functionalization (DF), respectively, on LPG were selected here as homomultivalent ligands for targeting HAs. Contrary to HA, the distribution of NA on the IAV surface is not uniform and highly variable. The tetrameric NAs are usually present on the virus surface as clusters of two or more proteins,[26] and previous reports showed that up to 10% ZA on a polymer backbone is enough to afford an effective inhibition of virus release from the cell surface.[28] We therefore prepared homomultivalent ZA on LPG with low (10%) and medium (40%) DFs, *i.e.*, $LPG_{10}ZA_{0.10}$ and $LPG_{10}ZA_{0.40}$, respectively. To achieve a favorable configuration for effective virus inhibition in the dual action mode, LPGs with optimum SA or SL and variable ZA densities were synthesized. Essential steps for the synthesis of ZA-alkyne are shown in Scheme 1A (for complete syntheses of ZA-alkyne and SL-alkyne, see Scheme S1 and S2). The DFs of each ligand on the heteromultivalent constructs correspond to the DF on the homomultivalent constructs to afford three heteromultivalent compounds, *i.e.*, $LPG_{10}ZA_{0.10}SA_{0.40}$, $LPG_{10}ZA_{0.10}SL_{0.40}$, and $LPG_{10}ZA_{0.40}SL_{0.40}$ (Scheme 1B and C, see the Supporting Information for details). The loading of ZA and SA/SL ligands was determined by ^{1}H NMR analysis, and the ζ-potentials of polymer conjugates were measured in PB (10 mM, pH 7.4) (Table 1), as well as in 10% DMEM and in 10% FBS to simulate the microenvironments of infection assays and cell culture mediums, respectively (Table S2).

We first tested the NA inhibition activity of all compounds against A/X31 (H3N2) in a standard fluorescence-based assay using 2′-(4-methylumbelliferyl)-α-D-*N*-acetylneuraminic acid (MUNANA) (Table 1, Figure 1A). The multivalent ZA compounds with different loadings of ZA alone ($LPG_{10}ZA_{0.10}$ and $LPG_{10}ZA_{0.40}$) or in combination with SA ($LPG_{10}ZA_{0.10}SA_{0.40}$) showed very low IC_{50} values in the nanomolar range (1.4−68.6 nM ZA). Interestingly, $LPG_{10}ZA_{0.10}SL_{0.40}$ and $LPG_{10}ZA_{0.40}SL_{0.40}$, with SL and ZA, showed weak NA inhibition (IC_{50} > 250 nM ZA), being almost 180× less efficient than the corresponding $LPG_{10}ZA_{0.10}SA_{0.40}$ (IC_{50} ∼ 1.4 nM ZA). This might be due to the reduced accessibility of randomly distributed ZA residues to the NA enzyme receptor pocket in the presence of the bulky trisaccharide units of SL residues on the same polymer chain. In this assay, where NA inhibition values solely depend on the NA binding, monovalent ZA has better NA inhibition than the multivalent analogs. These results might be attributed to the higher conformational entropic cost of grafted ZAs compared to free monovalent ZA ligands for making bound ZA-NA interaction pairs, as observed by others.[29] The control compound $LPG_{10}OH$ and sialic acid−based inhibitors $LPG_{10}SA_{0.40}$ and $LPG_{10}SL_{0.50}$ did not show any inhibition of NA activity.

Next, we studied the potential of these compounds as inhibitors of virus−cell binding. The hemagglutination inhibition (HAI) assay was performed with different compounds using IAVs A/X31 (H3N2), A/Panama/2007/1999 (H3N2), A/Bayern/63/2009 (H1N1pdm), and A/California/7/2009 (H1N1pdm) (Figure 1B). $LPG_{10}SA_{0.40}$ showed weak inhibitory activity only against H3N2 viruses, whereas $LPG_{10}SL_{0.40}$ also showed strong inhibition (K_i = 625 nM) of A/Bayern/63/2009. We expect an extended chain conformation of linear polyglycerol when conjugated with the trisaccharide SL ligands, thereby reducing the conformational penalty of the polymer for adsorption onto the virus surface as compared to the globular $LPG_{10}SA_{0.40}$. No globular morphologies were seen for $LPG_{10}SL_{0.50}$ in the cryo-TEM analysis (Figure S16). The heteromultivalent analogue $LPG_{10}ZA_{0.40}SL_{0.40}$ showed broad HA inhibition with low nM inhibition constants (K_i) against all tested IAV strains (Table S1). The ZA functionalized inhibitors ($LPG_{10}ZA_{0.10}$ and $LPG_{10}ZA_{0.40}$) showed little or no HA inhibition, and the heteromultivalent $LPG_{10}ZA_{0.10}SA_{0.40}$ inhibited hemagglutination substantially better than the homomultivalent $LPG_{10}SA_{0.40}$ only against A/X31. These data clearly show that the presence of ZA ligands leads to better virus inhibition. As described earlier, the multivalent polymer adsorption onto the receptor-coated virus surface depends on the conformation penalty of polymer and ligand−receptor pair interactions upon binding.[29,30] No HA inhibition was observed with control compounds $LPG_{10}OH$, zanamivir, and 6′-sialyllactose (Table S1).

To compare the broad therapeutic activity of different homo- and heteromultifunctional compounds against virus propagation in a multicyclic infection setup, we included the more recent virus of the H3N2 subtype, *i.e.*, A/Panama/2007/2009 and the pandemic H1N1 A/Bayern/63/2009, which diverge greatly from A/X31 on the HA and NA amino acid sequence (Figure 2). Compounds at different dilutions were incubated with Madin−Darby canine kidney (MDCK-II) cells

https://doi.org/10.1021/acs.nanolett.3c00408
Nano Lett. 2023, 23, 4844−4853

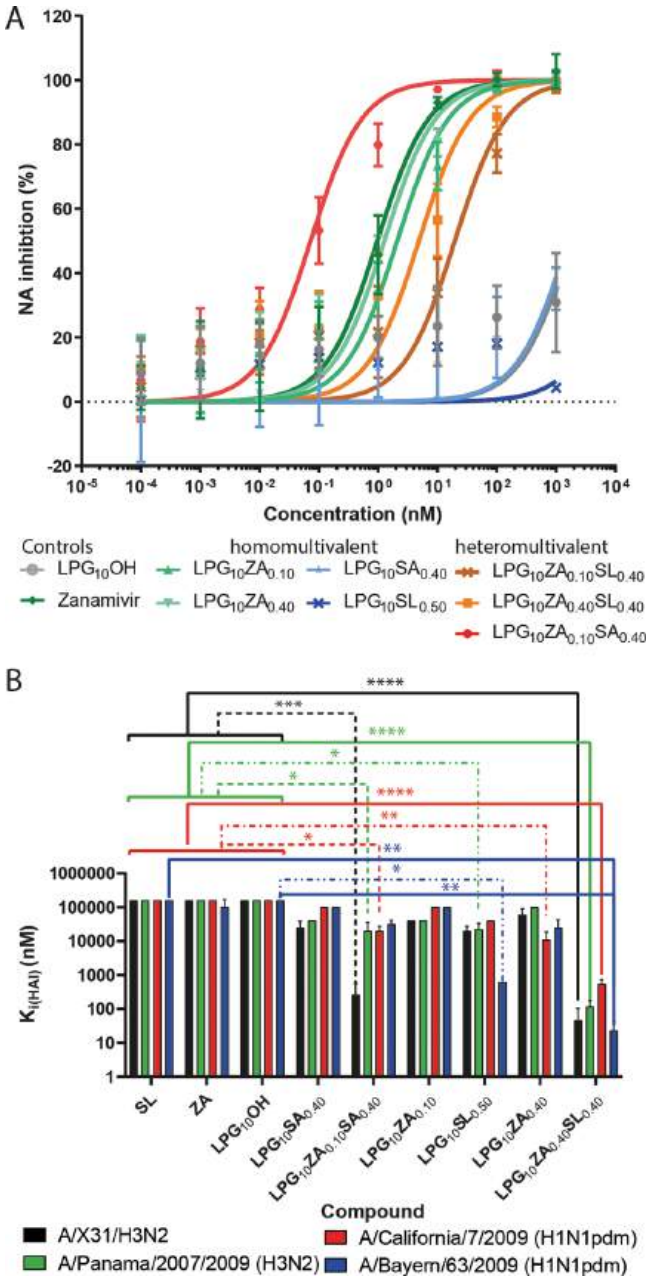

Figure 1. (A) NA inhibitory activity of the compounds determined using the MUNANA assay. Values are expressed as mean ± SD, $n = 6$. (B) Inhibitory effect of compounds tested against different IAV subtype strains. The inhibition constant $K_{i(HAI)}$ was calculated and presented as $\log_{10} K_{i(HAI)}$ for better visualization. The $K_{i(HAI)}$ reflects the lowest inhibitor concentration necessary to achieve full inhibition of virus-induced hemagglutination. The graph shows the mean and standard deviation (SD) of three independent experiments with each virus. *p*-values were determined using ANOVA with multiple testing (Kruskal–Wallis test and Dunn's test).

after establishing infection with the virus for 45 min at MOI 0.01. At 24 hpi, the virus titer in the supernatant was analyzed using a plaque assay. $LPG_{10}OH$ did not show any inhibition of virus propagation even at 1 or 10 μM, and SA-functionalized $LPG_{10}SA_{0.40}$ was active only against A/X31 with an IC_{50} of 31 nM (~1870 nM SA). A broader antiviral activity was observed when SA was replaced with SL residues that closely mimic the canonical receptor for IAV,[31] but IC_{50} values increased to 600–2800 nM. Commercially available monovalent ZA showed weak antiviral activity against all three strains (IC_{50} 6.5–9.9 μM). In contrast, multivalent ZA compounds $LPG_{10}ZA_{0.10}$ and $LPG_{10}ZA_{0.40}$, respectively, showed nanomolar IC_{50} values against A/X31 (6 and 3 nM) and A/Panama/2007/1999 (58 and 45 nM) but very high μM IC_{50} values against A/Bayern/63/2009 (77 and 14 μM). However, MDCK-II cells express only low levels of α-2,6-linked Neu5Ac, the host cell receptor of human IAVs. Thus, there are fewer glycan receptors to retain progeny virus at the cell surface and therefore viruses are less dependent on NA activity in this setting.[32] Increased antiviral activity of multivalent ZA compared to monovalent ZA against A/X31 and Panama strains under these conditions is intriguing, especially considering the weaker NA inhibition activity of multivalent ZA than the monovalent ZA (Table 1). These findings suggest that steric effects play a role in addition to the inhibition of NA by the multivalent ZA compounds, where the polymer bound to NA through ZA might sterically hinder the attachment of the virus to host cells. The steric inhibition of the virus surface has been discussed earlier.[24,33−36] As a result of steric shielding, larger multivalent objects that can display an otherwise similar or even smaller dissociation constant with a certain receptor compared to smaller ones might better prevent virus attachment to a cell and thus have higher viral inhibition because their larger size shields a larger number of viral receptors, preventing them from binding ligands on the host cell.

Using heteromultivalent inhibitors with both ZA and SA or SL on the same polymer chain effectively increased the inhibition of virus propagation, as indicated by a dramatic decrease in IC_{50} values. $LPG_{10}ZA_{0.10}SA_{0.40}$ demonstrated broad antiviral activity in a nM range against all three strains 0.2–156 nM (corresponding to 2 nM–2 μM ZA). Using SL residues instead of SA in combination with ZA ($LPG_{10}ZA_{0.40}SL_{0.40}$) further decreased the IC_{50} values to 0.7–2.0 nM (corresponding to 35–128 nM ZA). Interestingly, the dose–response curves for the virus propagation indicated that, in comparison to homomultivalent ZA analogs, the heteromultivalent SA and ZA improved the inhibition of propagation of A/Panama/2007/1999 slightly and A/Bayern/63/2009 significantly, although these viruses were not inhibited as much by the homomultivalent sialoside compound (Figure 2B and C). This may in part be explained by an earlier observation for A/Panama/2007/1999 showing that multivalent SA-functionalized polyglycerols can bind to virions without inhibiting their propagation.[23] The SA-supported binding of heteromultivalent LPG may contribute to a higher surface concentration of ZA and thus to an enhanced inhibitory effect of ZA.

Intriguingly, the dose–response curves of SL-containing compounds $LPG_{10}ZA_{0.40}SL_{0.40}$ and $LPG_{10}SL_{0.50}$ are much steeper than those of the SA-conjugated compounds for A/Panama/2007/1999 and A/Bayern/63/2009. For A/X31, homomultivalent $LPG_{10}SA_{0.40}$ caused a steeper dose response curve than $LPG_{10}SL_{0.50}$ (Figure 2A–C). This difference in steepness cannot be attributed to different degrees of ligand conjugation, as they are similar or at least in the same range for all compounds. It is conceivable that the length of the trisaccharide SL linker might also enhance the number of interacting HA molecules that are not accessible to a sole monosaccharide SA functionalization. In addition, SLs of the LPG not engaged in HA interaction may protrude from the viral surface and therefore may add to the steric inhibition.[36,37]

https://doi.org/10.1021/acs.nanolett.3c00408
Nano Lett. 2023, 23, 4844–4853

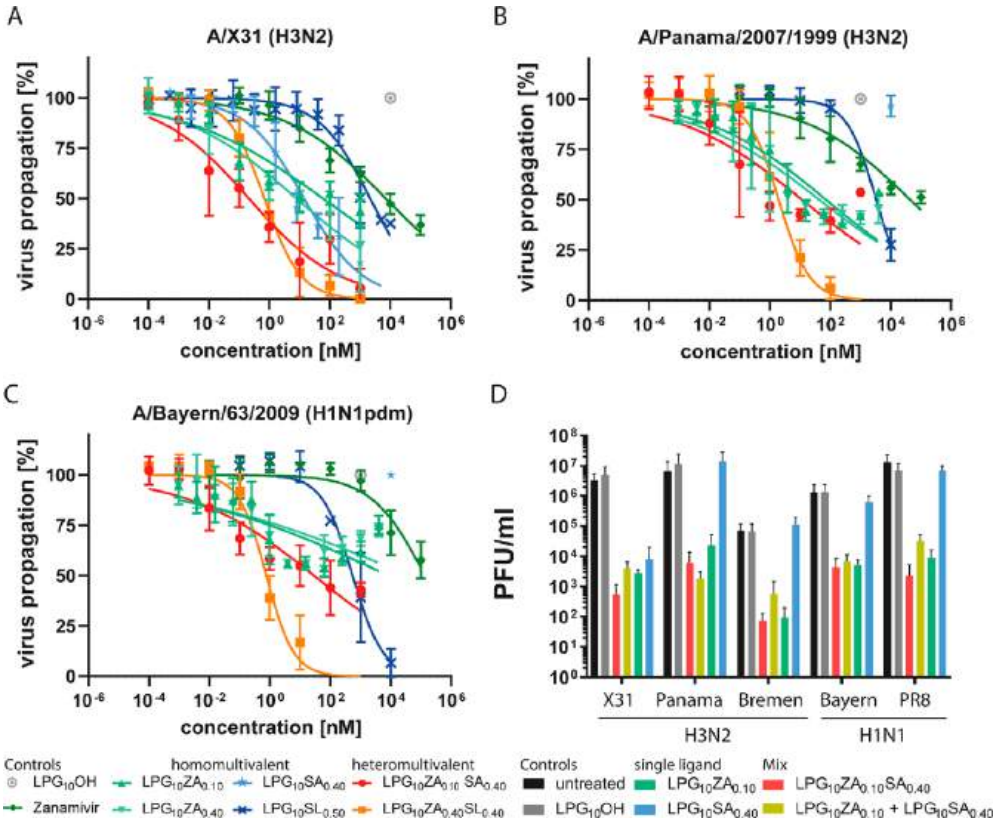

Figure 2. Investigation of different compounds in a multicyclic infection set up against different strains of the influenza A virus. Reduction in the virus titer in the presence of different compounds at different concentrations against the influenza viruses (A) A/X31 (H3N2), (B) A/Panama/2007/1999 (H3N2), and (C) A/Bayern/63/2009 (H1N1pdm), respectively. IC_{50} values in Table 2 were calculated from these curves using a four-order nonlinear regression fit in Graphpad Prism. (D) Reduction in virus titers of different strains (additionally including A/Bremen/5/2017 (H3N2) and A/PR/8/34 (H1N1)) at 10 nM of the compound using homomultivalent ZA and SA compounds as well as the physical mixture of homomultivalent LPG to compare to covalently bound heteromultivalent ligands. $LPG_{10}ZA_{0.10}SA_{0.40}$ at 10 nM corresponds to 130 nM ZA and 530 nM SA. A physical mixture containing 130 nM ZA in $LPG_{10}ZA_{0.10}$ and 530 nM SA in $LPG_{10}SA_{0.40}$ was used in the same experimental setting. Only the location names are used to refer to the different strains for clarity. All data represent three independent experiments in duplicate.

Table 2. Inhibition of Propagation of Diverse IAV Virus Strains in Cell Culture by Different Compounds[a]

	IC_{50} ± SD [nM] (SA, ZA)		
compounds	A/X31 (H3N2)	A/Panama/2007/2009 (H3N2)	A/Bayern/63/2009 (H1N1)
$LPG_{10}OH$			
$LPG_{10}SA_{0.40}$	31.17 ± 38.36 (SA 1870)	ND	ND
$LPG_{10}SL_{0.50}$	2841.67 ± 1223.89 (SL 190 391)	2400.33 ± 1475.07 (SL 160 822)	648.23 ± 459.69 (SL 43 431)
zanamivir	7282.00 ± 3733.91	9886.67 ± 5838.55	6537.00 ± 9244.71
$LPG_{10}ZA_{0.10}$	5.88 ± 3.02 (ZA 76)	58.46 ± 22.62 (ZA 760)	(7.72 ± 7.44) × 10^4 (ZA 1000 000)
$LPG_{10}ZA_{0.40}$	3.35 ± 0.57 (ZA 181)	45.47 ± 26.57 (ZA 2455)	(1.40 ± 1.71) × 10^4 (ZA 756 000)
$LPG_{10}ZA_{0.10}SA_{0.40}$	0.15 ± 0.08 (ZA 2, SA 9)	26.16 ± 38.21 (ZA 340, SA 1569)	156.18 ± 246.41 (ZA 2030, SA 9370)
$LPG_{10}ZA_{0.40}SL_{0.40}$	0.65 ± 0.36 (ZA, SL35)	2.37 ± 2.24 (ZA, SL 128)	0.86 ± 0.48 (ZA, SL 46)

[a]All compounds were added to the culture medium directly after 45 min of infection at MOI 0.01. IC_{50} values were calculated by fitting the data from Figure 2A–C using a four-order nonlinear regression. IC_{50} values are given as particle concentrations. In addition, the concentrations of the respective ligands are given in parentheses. ND = not detected.

The IC_{50} values of monovalent and homomultivalent zanamivir were much higher against A/Bayern/63/2009 than against the tested H3N2 viruses, implying the decreased zanamivir sensitivity of this virus. The heteromultivalent compounds were able to overcome this decreased zanamivir sensitivity, suggesting they might be suited to treat infections with NA inhibitor-resistant viruses as well. Overall, the heteromultivalent compound with both ZA and SL ligands, $LPG_{10}ZA_{0.40}SL_{0.40}$, was the most effective compound and accomplished >99.9% inhibition of virus propagation against the diverse IAVs tested, demonstrating its high potential for broad activity (Figure 2A–C). Important to note is that the presence of ZA–NA pairs on the virus surface might also stabilize HA–SL pairs, leading to long-lasting adsorption of heteromultivalent $LPG_{10}ZA_{0.40}SL_{0.40}$ and consequently better steric inhibition of the virus surface compared to its homomultivalent analogs.

To investigate if there was an added benefit of having both SA and ZA on the same polymer backbone in contrast to separate ones, a comparison of the heteromultivalent

https://doi.org/10.1021/acs.nanolett.3c00408
Nano Lett. 2023, 23, 4844–4853

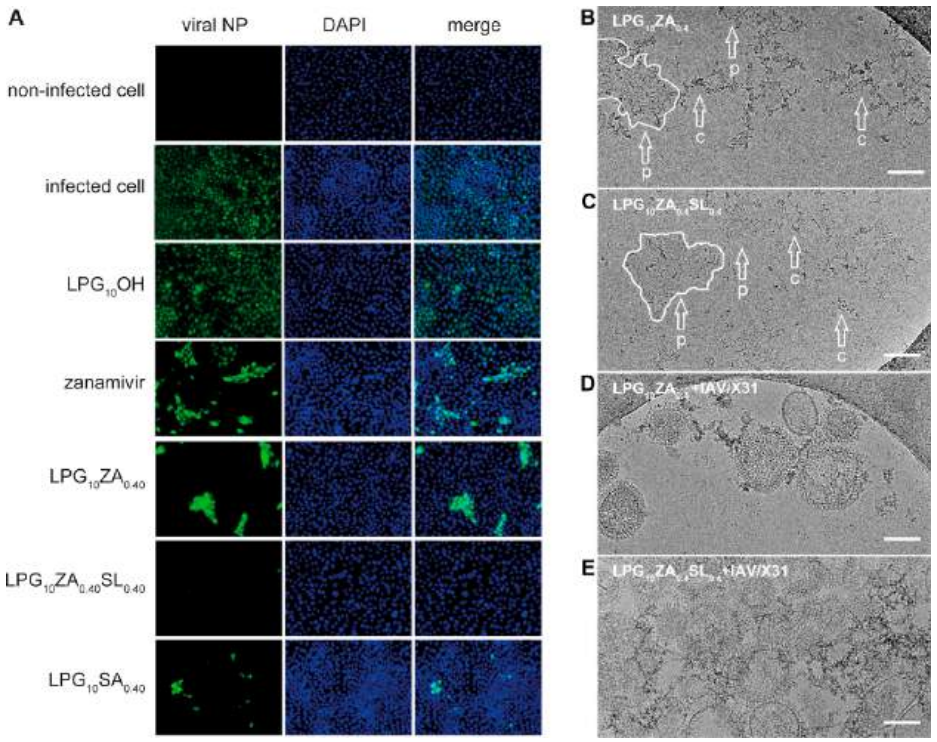

Figure 3. (A) Representative fluorescence images for infected cells being treated with the inhibitors. The cells were infected by IAV A/X31 (H3N2) for 45 min and then cultured in the medium containing 10 nM inhibitors for 24 h. The scale bar represents 50 μm. Immunostaining was done for the viral nucleoprotein (NP). More images are shown in Figure S21. Morphology of (B) $LPG_{10}ZA_{0.40}$ and (C) $LPG_{10}ZA_{0.40}SL_{0.40}$ (1 mM) embedded in vitreous ice. Arrows in (B) and (C) indicate condensed LPG structures (c) or planar 2D structures (p), the latter of which is partly outlined with a line. (D) Cryo-electron micrograph of $LPG_{10}ZA_{0.40}$ and (E) $LPG_{10}ZA_{0.40}SL_{0.40}$ incubated with IAV A/X31 (H3N2) in PBS pH 7.4 for 45 min at room temperature and embedded in vitreous ice. The scale bar corresponds to 100 nm.

$LPG_{10}ZA_{0.10}SA_{0.40}$ with the physical mixture of $LPG_{10}ZA_{0.10}$ and $LPG_{10}SA_{0.40}$ was performed in the multicyclic infection setup as above at a low inhibitor concentration of 10 nM. We observed for A/X31, A/Bremen/5/2017, and A/PR/8/34 that the heteromultivalent compound reduced the virus titer by one order of magnitude more than the physical mixture of the analogs (Figure 2D). The lower effect of physical mixtures might be attributed to the shielding effect,[24,33,36] which is posed by the homomultivalent analog once bound to the virus particle. For example, LPGSA once bound to the virus particle might also shield NAs and make them less accessible to binding with LPGZA analogs and vice versa. However, this warrants more detailed studies in the future. Importantly, no compounds showed any toxicity against MDCK-II cells in the MTS assay up to 10 μM concentration (Figure S19).

We imaged cells at 24 hpi with A/X31 in the presence of different inhibitors. Influenza A/X31 viral nucleoproteins (NPs) were labeled with antibodies to reveal infected cells, and DAPI staining of nuclei was used to mark the cells (representative images see Figures 3A and S20). In the infection control (absence of any LPG compound) and $LPG_{10}OH$-treated cells, almost all cells were infected within 24 hpi (MOI = 0.01). Upon the addition of polymeric inhibitors to the cell culture medium directly after 45 min of infection, the number of infected cells became substantially reduced. The heteromultivalent $LPG_{10}ZA_{0.40}SL_{0.40}$ showed significantly higher inhibitory activity than the two homomultivalent inhibitors ($LPG_{10}ZA_{0.40}$ and $LPG_{10}SA_{0.40}$). Similar to the IC_{50} analysis, we saw higher antiviral activities for multivalent zanamivir compounds ($LPG_{10}ZA_{0.10}$ and $LPG_{10}ZA_{0.40}$) over monomeric zanamivir. These findings demonstrate that attaching both HA and NA inhibitors to the same polymeric chain confers additional benefits for inhibiting virus spread and propagation even postinfection.

To visualize the IAV interactions, we did cryo-TEM imaging with different compounds at 1 mM concentrations and A/X31 (Figure S12–S16). The $LPG_{10}ZA_{0.10}$ showed clusters of thread-like structures and some 2D planar morphologies that were particularly evident in micrographs taken using a contrast-enhancing volta phase plate (Figures 3B and S12). The 2D planar morphologies were more prominent in $LPG_{10}ZA_{0.40}$ with increased loading of the ZA ligand that has both a positively charged guanidinium and a negatively charged carboxylate ion. The $LPG_{10}ZA_{0.40}$ carries a more negative ζ-potential (-17.41 ± 3.48 mV) than $LPG_{10}ZA_{0.10}$ ($\zeta = -3.31 \pm 1.40$ mV) (Table 1 and Figures S13 and S14) but a less negative ζ-potential than $LPG_{10}SA_{0.40}$ ($\zeta = -30$ mV). We hypothesize that the electrostatic interactions among different polymer chains are the main cause of the formation of 2D planar morphologies. The multivalent sialyllactose compound $LPG_{10}SL_{0.50}$ showed only some punctual or thread morphologies, which could be well recognized in stereo images (Figure S16). The heteromultivalent compound $LPG_{10}ZA_{0.40}SL_{0.40}$ showed 2D planar morphologies attributed to the presence of high ZA loading (Figure 3C and Figure S15).

We incubated the two most potent compounds $LPG_{10}ZA_{0.40}$ and $LPG_{10}ZA_{0.40}SL_{0.40}$ with A/X31 and plunge froze them for the cryo-TEM study. Interestingly, in the presence of the virus, 2D planar morphologies could not be recognized. The disruption of 2D structures might be because of the higher

https://doi.org/10.1021/acs.nanolett.3c00408
Nano Lett. 2023, 23, 4844−4853

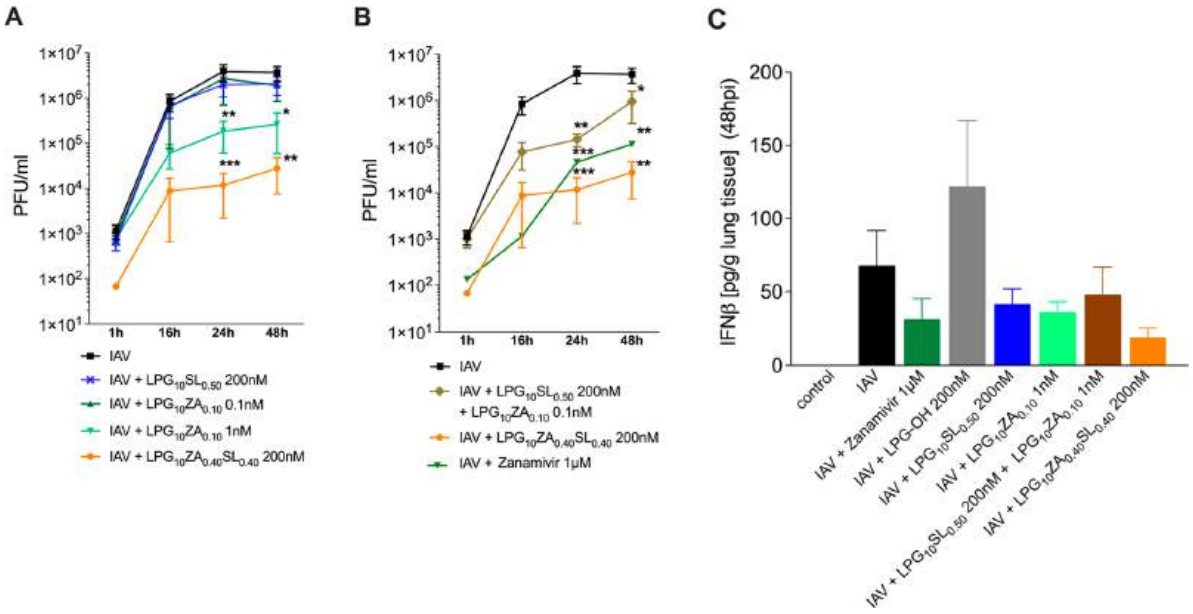

Figure 4. Inhibition of *ex vivo* human lung tissue influenza A virus A/Panama/2007/1999 (H3N2) propagation with different compounds. IAV (black) replication was compared to the replication after treatment with (A) $LPG_{10}SL_{0.50}$ (blue), $LPG_{10}ZA_{0.10}$ (green), or $LPG_{10}ZA_{0.40}SL_{0.40}$ (orange); (B) $LPG_{10}SL_{0.50}$ + $LPG_{10}ZA_{0.10}$ (brown) and $LPG_{10}ZA_{0.40}SL_{0.40}$ (orange); or (C) zanamivir (green). (D) Released IFN-β measured at 48 hpi. The control is the sample without any virus where no detectable IFN-β was released. Data are presented as the mean with SEM ($N = 4$). Data were analyzed using two-way ANOVA (*$p < 0.05$, **$p < 0.01$ ***$p < 0.001$, Dunnett's multiple comparisons test).

affinity of carbohydrate ligands toward viral proteins as compared to their potential electrostatic interactions among the ligands. The disruption of various noncovalent interactions, including electrostatic, H-bonding, or van der Waals, within or between sugar-conjugated polymer chains upon interaction with proteins has been known.[38,39] For example, Santos et al. reported the reorganization of glycosylated surfaces of vesicles upon interaction with lectin molecules.[40]

Some clusters of $LPG_{10}ZA_{0.40}$ in the vicinity of virions could be seen (Figures 3D and S17). For the most potent heteromultivalent compound $LPG_{10}ZA_{0.40}SL_{0.40}$, we observed a high virus density often surrounded by compound clusters, suggesting compound-mediated aggregation of virus particles (Figure 3E and Figure S18). This clustering effect may contribute to the efficient inhibition of virus propagation observed *in vitro* (Figures 1 and 2) and *ex vivo* (Figure 4).

To mimic the natural setting of the human lung, virus infections were studied in explanted human lung tissue infected *ex vivo*. Compounds were administered only once at 1.5 hpi with A/Panama/2007/1999 (0.4×10^6 PFU/mL), and plaque-forming units (PFU) in the supernatants of infected human lung tissue were assessed at 16, 24, and 48 hpi. The concentrations of different compounds with different degrees of functionalization were based on the previous *in vitro* assays and *ex vivo* optimization. A comparison of $LPG_{10}SL_{0.50}$ at 100 and 200 nM showed that at least a 200 nM concentration was required to observe a slight reduction in the virus titer (Figure S21). Similarly, $LPG_{10}ZA_{0.10}$ at 1 nM reduced the virus titer up to one order of magnitude within 48 hpi, whereas the 0.1 nM concentration was only slightly effective. Interestingly, a mixture of 0.1 nM $LPG_{10}ZA_{0.10}$ and 200 nM $LPG_{10}SL_{0.50}$ reduced the virus titer up to one order of magnitude at 16 and 24 h, but infectivity was restored within 48 hpi. Most effective was the heteromultivalent $LPG_{10}ZA_{0.40}SL_{0.40}$, which reduced the titer almost up to three orders of magnitude, and a plateau in PFU was reached at 16 hpi at 200 nM. Commercially available ZA was initially able to reduce virus titers when applied at μM concentration, although virus titers continued to rise steadily without reaching a plateau within 48 hpi (Figure 4A–C).

Taken together, the heteromultivalent compound $LPG_{10}ZA_{0.40}SL_{0.40}$ outperformed even physical mixtures of the highly active homomultivalent ZA and SL compounds *ex vivo*. The synergistic effect of SL and ZA of the heteromultivalent $LPG_{10}ZA_{0.40}SL_{0.40}$ is likely caused by a strong affinity of the ZA moiety for the viral NA, which in turn synergistically improves the binding of the SL moiety to the HA (and/or NA) protein of the same virus. Once bound, the polymer compound is also likely to inhibit nearby IAV surface proteins sterically, as is also the case for HA stem-binding antibodies[41] inhibiting sterically viral NAs, as well as accounting for the inhibition of virus release from the infected cell. The control compound $LPG_{10}OH$ without any ligand did not have any inhibition (Figure S21).

As a representative of antiviral cytokine release from infected cells at 48 hpi, we measured the level of IFN-β using ELISA. The levels of IFN-β were substantially reduced in infected tissue cultures treated with monovalent ZA of homomultivalent or heteromultivalent compounds. Furthermore, the IFN-β reduction was even more pronounced in the presence of the heteromultivalent compounds than other multivalent compounds or ZA alone (Figure 4D). Considering IFN-β as a representative interferon allows the assumption that the high antiviral activity of heteromultivalent compounds is mediated by their binding to viruses and not by cytokine induction.

In conclusion, the heteromultivalent polymer carrying SL and ZA units exhibits significantly higher antiviral effects than its homomultivalent analogs. It is also effective against those IAV strains for which the homomultivalent compounds show little to no effect, suggesting a potential application also against NA inhibitor-resistant strains. Overall, the high efficacy of the heteromultivalent polymer is not solely because of its

https://doi.org/10.1021/acs.nanolett.3c00408
Nano Lett. 2023, 23, 4844−4853

interaction with two different proteins on the virus surface but is a result of its better polymer adsorption and steric inhibition of the virus surface. The most potent $LPG_{10}ZA_{0.40}SL_{0.40}$ inhibits propagation of a broad variety of IAV strains up to >99.9% postinfection at a very low nM concentration and outperforms the commercial zanamivir drug *in vitro* and *ex vivo*. We demonstrate that the dual-action approach can be integrated into a small multivalent polymer, and it possesses a high potential to advance our options to combat IAV infections. This approach may also be applicable to combating infections with other viruses anchoring specific surface proteins.

■ ASSOCIATED CONTENT

Supporting Information

The Supporting Information is available free of charge at https://pubs.acs.org/doi/10.1021/acs.nanolett.3c00408.

Materials and methods, detailed synthetic protocols and reaction schemes, protocols for the biological assays, NMR figures, cryo-TEM and confocal images, cytotoxicity analysis, *ex vivo* infection inhibition plots, hemagglutination inhibition data using different IAV strains, and ζ-potential data(PDF)

■ AUTHOR INFORMATION

Corresponding Author

Sumati Bhatia − *Institut für Chemie und Biochemie Organische Chemie, Freie Universität Berlin, 14195 Berlin, Germany;* orcid.org/0000-0002-5123-4937; Email: sumati@zedat.fu-berlin.de

Authors

Badri Parshad − *Institut für Chemie und Biochemie Organische Chemie, Freie Universität Berlin, 14195 Berlin, Germany; Wellman Center for Photomedicine, Massachusetts General Hospital, Harvard Medical School, Boston, Massachusetts 02129, United States;* orcid.org/0000-0001-6496-8844

Marlena N. Schlecht − *Unit 17, Influenza and Other Respiratory Viruses, Robert Koch-Institut, 13353 Berlin, Germany; Medical Clinic III, Division of Nephrology, Medizinische Fakultät Carl Gustav Carus an der TU Dresden, 01307 Dresden, Germany;* orcid.org/0000-0001-8893-5326

Morris Baumgardt − *Department of Infectious Diseases, Respiratory Medicine and Critical Care, Charité−Universitätsmedizin Berlin, Corporate Member of Freie Universität Berlin and Humboldt-Universität zu Berlin, 10117 Berlin, Germany*

Kai Ludwig − *Forschungszentrum für Elektronenmikroskopie and Core Facility BioSupraMol, Institut für Chemie und Biochemie, Freie Universität Berlin, 14195 Berlin, Germany*

Chuanxiong Nie − *Institut für Chemie und Biochemie Organische Chemie, Freie Universität Berlin, 14195 Berlin, Germany*

Agustina Rimondi − *Unit 17, Influenza and Other Respiratory Viruses, Robert Koch-Institut, 13353 Berlin, Germany*

Katja Hönzke − *Department of Infectious Diseases, Respiratory Medicine and Critical Care, Charité−Universitätsmedizin Berlin, Corporate Member of Freie Universität Berlin and Humboldt-Universität zu Berlin, 10117 Berlin, Germany*

Stefano Angioletti-Uberti − *Department of Materials, Imperial College London, London SW7 2AZ, U.K.*

Vinod Khatri − *Institut für Chemie und Biochemie Organische Chemie, Freie Universität Berlin, 14195 Berlin, Germany*

Paul Schneider − *Department for Thoracic Surgery, DRK Clinics, 13359 Berlin, Germany*

Andreas Herrmann − *Institut für Chemie und Biochemie Organische Chemie, Freie Universität Berlin, 14195 Berlin, Germany*

Rainer Haag − *Institut für Chemie und Biochemie Organische Chemie, Freie Universität Berlin, 14195 Berlin, Germany*

Andreas C. Hocke − *Department of Infectious Diseases, Respiratory Medicine and Critical Care, Charité−Universitätsmedizin Berlin, Corporate Member of Freie Universität Berlin and Humboldt-Universität zu Berlin, 10117 Berlin, Germany*

Thorsten Wolff − *Unit 17, Influenza and Other Respiratory Viruses, Robert Koch-Institut, 13353 Berlin, Germany;* orcid.org/0000-0001-7688-236X

Complete contact information is available at: https://pubs.acs.org/10.1021/acs.nanolett.3c00408

Author Contributions

$^{\nabla}$B.P. and M.N.S. contributed equally to this work.

Notes

The authors declare no competing financial interest.

■ ACKNOWLEDGMENTS

The authors acknowledge financial support by the Collaborative Research Center 765 and 1449 of the Deutsche Forschungsgemeinschaft (DFG) and Berlin University Alliance (BUA). S.B. acknowledges funding from DFG project no. 458564133. K.H. and A.C.H. were supported by DFG (SFB-TR 84). K.H. and A.C.H. were funded by BMBF (NUM-COVID 19, Organo-Strat 01KX2021), and A.C.H. was funded by BMBF (RAPID) and Berlin University Alliance GC2 Global Health (Corona Virus Pre-Exploration Project). M.B., K.H., and A.C.H. were supported by Einstein Foundation EC3R. We acknowledge Stefan Hippenstiel for his valuable advice on human lung explant experiments. A.R. is funded by the Alexander von Humboldt Foundation.

■ REFERENCES

(1) *Influenza (Seasonal)*. World Health Organization, January 12, 2023.https://www.who.int/news-room/fact-sheets/detail/influenza-(seasonal).

(2) Mahase, E. H5N1: Has There Been Human-to-Human Transmission, and Do We Have a Vaccine? *BMJ*. **2023**, p510.

(3) Bai, L.; Zhao, Y.; Dong, J.; Liang, S.; Guo, M.; Liu, X.; Wang, X.; Huang, Z.; Sun, X.; Zhang, Z.; Dong, L.; Liu, Q.; Zheng, Y.; Niu, D.; Xiang, M.; Song, K.; Ye, J.; Zheng, W.; Tang, Z.; Tang, M.; Zhou, Y.; Shen, C.; Dai, M.; Zhou, L.; Chen, Y.; Yan, H.; Lan, K.; Xu, K. Coinfection with Influenza A Virus Enhances SARS-CoV-2 Infectivity. *Cell Res.* **2021**, *31* (4), 395−403.

(4) Cuadrado-Payán, E.; Montagud-Marrahi, E.; Torres-Elorza, M.; Bodro, M.; Blasco, M.; Poch, E.; Soriano, A.; Piñeiro, G. J. SARS-CoV-2 and Influenza Virus Co-Infection. *Lancet* **2020**, *395* (10236), No. e84.

(5) Stowe, J.; Tessier, E.; Zhao, H.; Guy, R.; Muller-Pebody, B.; Zambon, M.; Andrews, N.; Ramsay, M.; Lopez Bernal, J. Interactions between SARS-CoV-2 and Influenza, and the Impact of Coinfection

on Disease Severity: A Test-Negative Design. *Int. J. Epidemiol* **2021**, *50* (4), 1124−1133.
(6) de Vries, E.; Du, W.; Guo, H.; de Haan, C. A. M. Influenza A Virus Hemagglutinin−Neuraminidase−Receptor Balance: Preserving Virus Motility. *Trends Microbiol* **2020**, *28* (1), 57−67.
(7) Vahey, M. D.; Fletcher, D. A. Influenza A Virus Surface Proteins Are Organized to Help Penetrate Host Mucus. *Elife* **2019**, *8*, No. e43764.
(8) Hamming, P. H.; Overeem, N. J.; Huskens, J. Influenza as a Molecular Walker. *Chem. Sci.* **2020**, *11* (1), 27−36.
(9) McAuley, J. L.; Gilbertson, B. P.; Trifkovic, S.; Brown, L. E.; McKimm-Breschkin, J. L. Influenza Virus Neuraminidase Structure and Functions. *Front Microbiol* **2019**, *10*, 1−13.
(10) Burckhardt, C. J.; Greber, U. F. Virus Movements on the Plasma Membrane Support Infection and Transmission between Cells. *PLoS Pathog* **2009**, *5* (11), No. e1000621.
(11) Overeem, N. J.; Vries, E.; Huskens, J. A Dynamic, Supramolecular View on the Multivalent Interaction between Influenza Virus and Host Cell. *Small* **2021**, *17* (13), 2007214.
(12) Cohen, M.; Zhang, X.-Q.; Senaati, H. P.; Chen, H.-W.; Varki, N. M.; Schooley, R. T.; Gagneux, P. Influenza A Penetrates Host Mucus by Cleaving Sialic Acids with Neuraminidase. *Virol J.* **2013**, *10*, 321.
(13) von Itzstein, M.; Dyason, J. C.; Oliver, S. W.; White, H. F.; Wu, W.-Y.; Kok, G. B.; Pegg, M. S. A Study of the Active Site of Influenza Virus Sialidase: An Approach to the Rational Design of Novel Anti-Influenza Drugs. *J. Med. Chem.* **1996**, *39* (2), 388−391.
(14) Trebbien, R.; Pedersen, S. S.; Vorborg, K.; Franck, K. T.; Fischer, T. K. Development of Oseltamivir and Zanamivir Resistance in Influenza A(H1N1)Pdm09 Virus, Denmark, 2014. *Euro Surveill* **2017**, *22* (3), 1−8.
(15) Mammen, M.; Dahmann, G.; Whitesides, G. M. Effective Inhibitors of Hemagglutination by Influenza Virus Synthesized from Polymers Having Active Ester Groups. Insight into Mechanism of Inhibition. *J. Med. Chem.* **1995**, *38* (21), 4179−4190.
(16) Kwon, S.-J.; Na, D. H.; Kwak, J. H.; Douaisi, M.; Zhang, F.; Park, E. J.; Park, J.-H.; Youn, H.; Song, C.-S.; Kane, R. S.; Dordick, J. S.; Lee, K. B.; Linhardt, R. J. Nanostructured Glycan Architecture Is Important in the Inhibition of Influenza A Virus Infection. *Nat. Nanotechnol* **2017**, *12* (1), 48−54.
(17) Papp, I.; Sieben, C.; Ludwig, K.; Roskamp, M.; Böttcher, C.; Schlecht, S.; Herrmann, A.; Haag, R. Inhibition of Influenza Virus Infection by Multivalent Sialic-Acid-Functionalized Gold Nanoparticles. *Small* **2010**, *6* (24), 2900−2906.
(18) Lauster, D.; Klenk, S.; Ludwig, K.; Nojoumi, S.; Behren, S.; Adam, L.; Stadtmüller, M.; Saenger, S.; Zimmler, S.; Hönzke, K.; Yao, L.; Hoffmann, U.; Bardua, M.; Hamann, A.; Witzenrath, M.; Sander, L. E.; Wolff, T.; Hocke, A. C.; Hippenstiel, S.; De Carlo, S.; Neudecker, J.; Osterrieder, K.; Budisa, N.; Netz, R. R.; Böttcher, C.; Liese, S.; Herrmann, A.; Hackenberger, C. P. R. Phage Capsid Nanoparticles with Defined Ligand Arrangement Block Influenza Virus Entry. *Nat. Nanotechnol* **2020**, *15* (5), 373−379.
(19) Bhatia, S.; Hilsch, M.; Cuellar-Camacho, J. L.; Ludwig, K.; Nie, C.; Parshad, B.; Wallert, M.; Block, S.; Lauster, D.; Böttcher, C.; Herrmann, A.; Haag, R. Adaptive Flexible Sialylated Nanogels as Highly Potent Influenza A Virus Inhibitors. *Angew. Chem., Int. Ed.* **2020**, *59* (30), 12417−12422.
(20) Kumari, M.; Prasad, S.; Fruk, L.; Parshad, B. Polyglycerol-Based Hydrogels and Nanogels: From Synthesis to Applications. *Future Med. Chem.* **2021**, *13* (4), 419−438.
(21) Wang, H.; Huang, W.; Orwenyo, J.; Banerjee, A.; Vasta, G. R.; Wang, L.-X. Design and Synthesis of Glycoprotein-Based Multivalent Glyco-Ligands for Influenza Hemagglutinin and Human Galectin-3. *Bioorg. Med. Chem.* **2013**, *21* (7), 2037−2044.
(22) Sauter, N. K.; Bednarski, M. D.; Wurzburg, B. A.; Hanson, J. E.; Whitesides, G. M.; Skehel, J. J.; Wiley, D. C. Hemagglutinins from Two Influenza Virus Variants Bind to Sialic Acid Derivatives with Millimolar Dissociation Constants: A 500-MHz Proton Nuclear Magnetic Resonance Study. *Biochemistry* **1989**, *28* (21), 8388−8396.
(23) Stadtmueller, M. N.; Bhatia, S.; Kiran, P.; Hilsch, M.; Reiter-Scherer, V.; Adam, L.; Parshad, B.; Budt, M.; Klenk, S.; Sellrie, K.; Lauster, D.; Seeberger, P. H.; Hackenberger, C. P. R.; Herrmann, A.; Haag, R.; Wolff, T. Evaluation of Multivalent Sialylated Polyglycerols for Resistance Induction in and Broad Antiviral Activity against Influenza A Viruses. *J. Med. Chem.* **2021**, *64* (17), 12774−12789.
(24) Bhatia, S.; Lauster, D.; Bardua, M.; Ludwig, K.; Angioletti-Uberti, S.; Popp, N.; Hoffmann, U.; Paulus, F.; Budt, M.; Stadtmüller, M.; Wolff, T.; Hamann, A.; Böttcher, C.; Herrmann, A.; Haag, R. Linear Polysialoside Outperforms Dendritic Analogs for Inhibition of Influenza Virus Infection in Vitro and in Vivo. *Biomaterials* **2017**, *138*, 22−34.
(25) Thomas, A.; Müller, S. S.; Frey, H. Beyond Poly(Ethylene Glycol): Linear Polyglycerol as a Multifunctional Polyether for Biomedical and Pharmaceutical Applications. *Biomacromolecules* **2014**, *15* (6), 1935−1954.
(26) Harris, A.; Cardone, G.; Winkler, D. C.; Heymann, J. B.; Brecher, M.; White, J. M.; Steven, A. C. Influenza Virus Pleiomorphy Characterized by Cryoelectron Tomography. *Proc. Natl. Acad. Sci. U. S. A.* **2006**, *103* (50), 19123−19127.
(27) Vahey, M. D.; Fletcher, D. A. Low-Fidelity Assembly of Influenza A Virus Promotes Escape from Host Cells. *Cell* **2019**, *176* (1−2), 281−294.e19.
(28) Masuda, T.; Yoshida, S.; Arai, M.; Kaneko, S.; Yamashita, M.; Honda, T. Synthesis and Anti-Influenza Evaluation of Polyvalent Sialidase Inhibitors Bearing 4-Guanidino-Neu5Ac2en Derivatives. *Chem. Pharm. Bull. (Tokyo)* **2003**, *51* (12), 1386−1398.
(29) Varilly, P.; Angioletti-Uberti, S.; Mognetti, B. M.; Frenkel, D. A General Theory of DNA-Mediated and Other Valence-Limited Colloidal Interactions. *J. Chem. Phys.* **2012**, *137* (9), 094108.
(30) Angioletti-Uberti, S.; Varilly, P.; Mognetti, B. M.; Tkachenko, A. V.; Frenkel, D. Communication: A Simple Analytical Formula for the Free Energy of Ligand−Receptor-Mediated Interactions. *J. Chem. Phys.* **2013**, *138* (2), 021102.
(31) de Graaf, M.; Fouchier, R. A. M. Role of Receptor Binding Specificity in Influenza A Virus Transmission and Pathogenesis. *EMBO J.* **2014**, *33* (8), 823−841.
(32) Hatakeyama, S.; Sakai-Tagawa, Y.; Kiso, M.; Goto, H.; Kawakami, C.; Mitamura, K.; Sugaya, N.; Suzuki, Y.; Kawaoka, Y. Enhanced Expression of an A2,6-Linked Sialic Acid on MDCK Cells Improves Isolation of Human Influenza Viruses and Evaluation of Their Sensitivity to a Neuraminidase Inhibitor. *J. Clin Microbiol* **2005**, *43* (8), 4139−4146.
(33) Mammen, M.; Choi, S.-K.; Whitesides, G. M. Polyvalent Interactions in Biological Systems: Implications for Design and Use of Multivalent Ligands and Inhibitors. *Angew. Chem., Int. Ed.* **1998**, *37* (20), 2754−2794.
(34) Vonnemann, J.; Liese, S.; Kuehne, C.; Ludwig, K.; Dernedde, J.; Böttcher, C.; Netz, R. R.; Haag, R. Size Dependence of Steric Shielding and Multivalency Effects for Globular Binding Inhibitors. *J. Am. Chem. Soc.* **2015**, *137* (7), 2572−2579.
(35) Dernedde, J.; Rausch, A.; Weinhart, M.; Enders, S.; Tauber, R.; Licha, K.; Schirner, M.; Zügel, U.; von Bonin, A.; Haag, R. Dendritic Polyglycerol Sulfates as Multivalent Inhibitors of Inflammation. *Proc. Natl. Acad. Sci. U. S. A.* **2010**, *107* (46), 19679−19684.
(36) Lees, W. J.; Spaltenstein, A.; Kingery-Wood, J. E.; Whitesides, G. M. Polyacrylamides Bearing Pendant Alpha.-Sialoside Groups Strongly Inhibit Agglutination of Erythrocytes by Influenza A Virus: Multivalency and Steric Stabilization of Particulate Biological Systems. *J. Med. Chem.* **1994**, *37* (20), 3419−3433.
(37) Ponader, D.; Maffre, P.; Aretz, J.; Pussak, D.; Ninnemann, N. M.; Schmidt, S.; Seeberger, P. H.; Rademacher, C.; Nienhaus, G. U.; Hartmann, L. Carbohydrate-Lectin Recognition of Sequence-Defined Heteromultivalent Glycooligomers. *J. Am. Chem. Soc.* **2014**, *136* (5), 2008−2016.
(38) Zeng, X.; Qu, K.; Rehman, A. Glycosylated Conductive Polymer: A Multimodal Biointerface for Studying Carbohydrate−Protein Interactions. *Acc. Chem. Res.* **2016**, *49* (9), 1624−1633.

https://doi.org/10.1021/acs.nanolett.3c00408
Nano Lett. 2023, 23, 4844−4853

(39) Mittal, A.; Krishna; Aarti; Prasad, S.; Mishra, P. K.; Sharma, S. K.; Parshad, B. Self-Assembly of Carbohydrate-Based Small Amphiphiles and Their Applications in Pathogen Inhibition and Drug Delivery: A Review. *Mater. Adv.* **2021**, *2* (11), 3459−3473.
(40) dos Santos, M. C.; Micheletto, Y. M. S.; da Silveira, N. P.; da Silva Pinto, L.; Giacomelli, F. C.; de Lima, V. R.; Frizon, T. E. A.; Dal-Bó, A. G. Self-Assembled Carbohydrate-Based Vesicles for Lectin Targeting. *Colloids Surf. B Biointerfaces* **2016**, *148*, 12−18.
(41) Kosik, I.; Angeletti, D.; Gibbs, J. S.; Angel, M.; Takeda, K.; Kosikova, M.; Nair, V.; Hickman, H. D.; Xie, H.; Brooke, C. B.; Yewdell, J. W. Neuraminidase Inhibition Contributes to Influenza A Virus Neutralization by Anti-Hemagglutinin Stem Antibodies. *J. Exp Med.* **2019**, *216* (2), 304−316.

https://doi.org/10.1021/acs.nanolett.3c00408
Nano Lett. 2023, 23, 4844−4853

Inhibitors Hot Paper

How to cite: *Angew. Chem. Int. Ed.* **2020**, *59*, 15532–15536
International Edition: doi.org/10.1002/anie.202004832
German Edition: doi.org/10.1002/ange.202004832

Topology-Matching Design of an Influenza-Neutralizing Spiky Nanoparticle-Based Inhibitor with a Dual Mode of Action

Chuanxiong Nie, Badri Parshad, Sumati Bhatia, Chong Cheng, Marlena Stadtmüller, Alexander Oehrl, Yannic Kerkhoff, Thorsten Wolff,* and Rainer Haag**

Abstract: *In this study, we demonstrate the concept of "topology-matching design" for virus inhibitors. With the current knowledge of influenza A virus (IAV), we designed a nanoparticle-based inhibitor (nano-inhibitor) that has a matched nanotopology to IAV virions and shows hetero-multivalent inhibitory effects on hemagglutinin and neuraminidase. The synthesized nano-inhibitor can neutralize the viral particle extracellularly and block its attachment and entry to the host cells. The virus replication was significantly reduced by 6 orders of magnitude in the presence of the reverse designed nano-inhibitors. Even when used 24 hours after the infection, more than 99.999 % inhibition is still achieved, which indicates such a nano-inhibitor might be a potent antiviral for the treatment of influenza infection.*

Besides the recent SARS-CoV-2 pandemic, outbreaks of seasonal or pandemic influenza A virus (IAV) have also challenged public health due to the high mutation rates of viral glycoprotein genes and the potential for human infection by animal strains.[1] Due to the lack of universal influenza vaccines, a robust virus-neutralizing therapeutic is needed.[2] IAV is an enveloped RNA virus, the membrane of which anchors two viral proteins that regulate interactions of the virion with the host cells, hemagglutinin (HA) and neuraminidase (NA).[3] For infection, IAV uses HA to bind to sialic acid on the host cell membrane. After completion of the replication cycle, the viral NA cleaves sialic acid from surface receptors to allow virion release, so-called budding.[4] Recent evidence also demonstrates that NA helps IAV penetration in the mucus by cleaving HA decoy receptors, which reveals the crucial role for a balanced HA/NA interplay for the binding behavior.[5] Multivalent sialylated nanostructures have been developed to inhibit HA and block viral entry to host cells.[6] However, heteromultivalent inhibitors engaging both HA and NA have been rarely been reported.[15]

From a topological viewpoint, the virion of IAV is nano-sized particle around 100 nm with a spiky surface generated by the HA and NA.[7] For an inhibitor, especially nanoparticle-based inhibitors (nano-inhibitors), matching the size and topology to the virion is essential in order to achieve robust binding to compete with the virus/cell interaction. For this purpose, flexible nanomaterials are favored to afford the viral binding ligands, but they also face the problem of overcoming the internal stress of the scaffold nanomaterials.[8] In our new approach, we used a rigid nanoparticle with a matching nanotopology to the viral particle, which binds more strongly than the flexible nanomaterials.[9]

The aim of this study was to develop a nano-inhibitor with the principle of topology-matching design. The inhibitor should not only show dual inhibitory effects on HA and NA, but should also exhibit a matched nanotopology to IAV virion, which is expected to increase the contact area and enhance the binding. To achieve that, a virus-like nanoparticle (VLNP) with nanospikes was first synthesized according to an earlier report.[10] Except for the difference of the morphology, the VLNP was the same as its smooth control nanoparticle for size and density (Figure S2 in the Supporting Information). Then, the nano-inhibitor was synthesized through the functionalization of the VLNP with linear polyglycerol-sialyllactose (LPG-SAL) and LPG-zanamivir (LPG-Zan) through copper-free SPAAC click reactions as shown in Figure 1 a. Despite the different subtypes of HA, human IAV strains tend to bind the 6′-sialyllactose for entry into host cells.[11] In this study, 6′-sialyllactose was conjugated onto the nanoparticles via an LPG linker in a multivalent manner as shown in Figure 1 b, since polyglycerol-based multivalent structures have been shown to efficiently to block virus infection in our former studies.[6c,d] In order to inhibit NA, an approved NA inhibitor, zanamivir, was also conjugated to the VLNPs, similarly in a multivalent manner.[12] The resulted hetero-multivalent structure is expected to bind IAV virion strongly as shown in Figure 1 c.

High-resolution TEM (HR-TEM) images were acquired to show the LPG-SAL and LPG-Zan conjugation on the VLNPs (Figure 1 d). The bare VLNPs had a rough surface with clear and sharp edges. With the conjugation of LPG-SAL

[*] C. Nie, Dr. S. Bhatia, Dr. A. Oehrl, Y. Kerkhoff, Prof. Dr. R. Haag
Institute of Chemistry and Biochemistry, Freie Universität Berlin
Takustr. 3, 14195 Berlin (Germany)
E-mail: chuanxnie@zedat.fu-berlin.de
haag@chemie.fu-berlin.de
C. Nie, M. Stadtmüller, Dr. T. Wolff
Unit 17, Robert Koch Institut, Seestr. 10, 13353 Berlin (Germany)
E-mail: WolffT@rki.de
Dr. B. Parshad
Department of Chemical Engineering and Biotechnology
University of Cambridge, Cambridge CB3 0AS (UK)
Prof. Dr. C. Cheng
College of Polymer Science and Engineering, Sichuan University
No.24 South Section 1, Yihuan Road, 610065, Chengdu (China)
Supporting information and the ORCID identification number(s) for the author(s) of this article can be found under: https://doi.org/10.1002/anie.202004832.

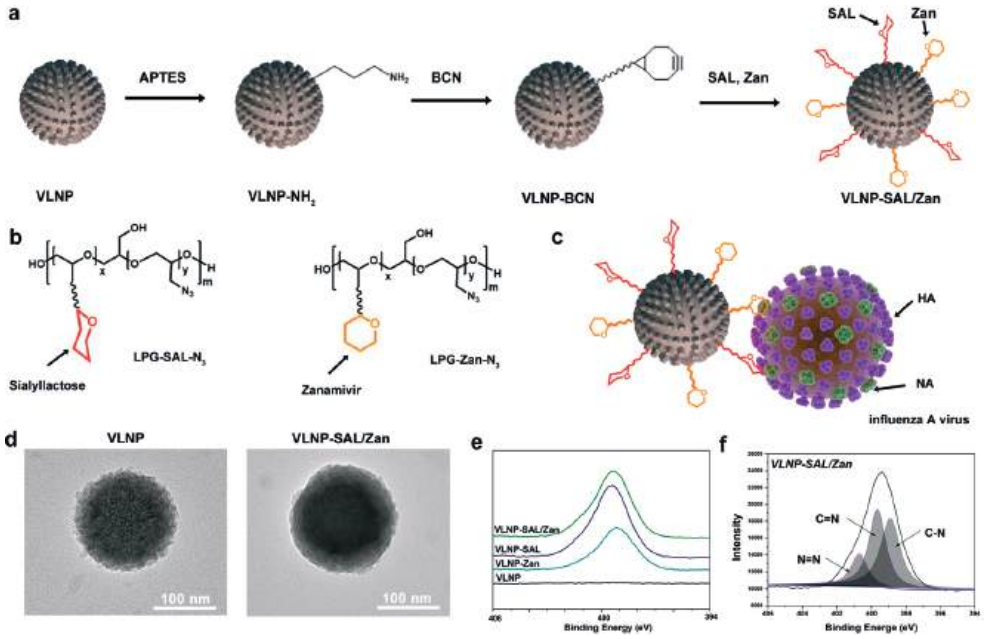

Figure 1. a) Synthetic outline for the topology-matching design of nano-inhibitors towards IAV. b) Structure of LPG-SAL-N_3 and LPG-Zan-N_3, which were used for the functionalization. Detailed structures are shown Figure S1. c) Proposed binding patterns between VLNP-SAL/Zan and influenza virus particles. d) HR-TEM images for the VLNPs before and after the functionalization. Scale bar: 100 nm. The images for smooth nanoparticle are shown in Figure S3. e) XPS N1s spectra for the VLNPs with the functionalization. f) Peak analysis for the XPS N1s spectra for VLNP-SAL/Zan.

and LPG-Zan, the spiky nanostructure is smoother, but a rough surface was still noticed, which shows advantages for the efficient binding of virus in the following studies. The chemical structure of VLNP-SAL/Zan was studied by XPS analysis, as shown in Figure 1 e,f. From the XPS N1s scan, the emerge of the N1s signal for VLNP-SAL/Zan indicated that the LPG-SAL and LPG-Zan have been conjugated to the VLNP. For the N1s scan, three characteristic peaks were detected as shown in Figure 1 e. Overall, the results of HR-TEM and XPS revealed that the VLNPs had been successfully functionalized with LPG-SAL and LPG-Zan.

Binding with the virus was studied by a centrifuge western blotting as shown in Figure 2 a,b and Figure S4, and the band intensity for the viral nucleoprotein (viral NP) reveals the amounts of virus binding to the nanoparticles. For the LPG-functionalized smooth nanoparticles (Figure S4), no binding was detected. But VLNP-LPG showed weak binding with the virus, which is likely due to the spiky nanostructures on the surface. All the SAL nanoparticles showed robust binding to influenza virus and VLNP-SAL/Zan was better than VLNP-SAL. This should be attributed to the additional interactions between Zan and NA, which not only added extra binding sites to the nanoparticles, but also enhanced the SAL/HA interaction.[13] It was also clear that the nanospikes on the surface have a positive effect on the viral binding. Cryo-TEM image was acquired to show the effect of the nanospikes on the viral binding as shown in Figure 2 c. From the images, it can be seen that the surface proteins can insert into the gaps of the nanospikes, which increased the contact area to benefit the binding. Furthermore, aggregates of the VLNP-SAL/Zan with the virus particles were also noticed.

NA inhibition was studied by MU-NANA assay (Figure 2 d). The nanoparticles with zanamivir all showed inhibition of NA and the $IC_{50(NA)}$ values for the VLNP-SAL/Zan, NP-SAL/Zan, and VLNP-Zan particles are 5.38 ± 1.37, 40.34 ± 10.82, $20.54 \pm 1.31\ \mu g\,mL^{-1}$, respectively. By comparing the results for VLNP-SAL/Zan and NP-SAL/Zan, an enhancement by a factor of 8 was also noticed for the spiky nanostructures, which can be attributed to increased virus binding by the spiky nanostructures.

We then investigated whether the binding of IAV virions to MDCK II cells can be blocked by the nano-inhibitors, to demonstrate that they act through a binding-decoy mechanism (Figure 3 a–c). In this test, virions of influenza A/X31 (H3N2) were labelled with octadecyl rhodamine B chloride (R18) and incubated with the nano-inhibitors for 45 minutes.[14] After being incubated for 45 minutes with the virion/inhibitor mixture, the cells were washed with PBS to remove free virus and then fixed for fluorescent microscopy (Figure 3 a) or harvested for flow cytometry (Figure 3 b). The results clearly show that the number of virions binding to the cells was reduced by the

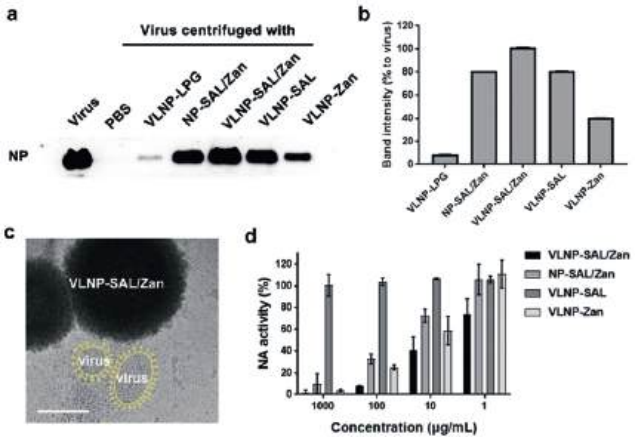

Figure 2. a) Western blot of influenza nucleoprotein (NP) that reveals viral binding to the nanoparticles.b) Band-intensity analysis for the western blot in (a). c) Cryo-EM images for virus binding to VLNP-SAL/Zan. The virus is marked yellow for a better view. Images without marks are shown in Figure S5. Scale Bar: 100 nm. d) Inhibition of NA activity by the nano-inhibitors. Values are expressed by mean ± SD, $n = 4$.

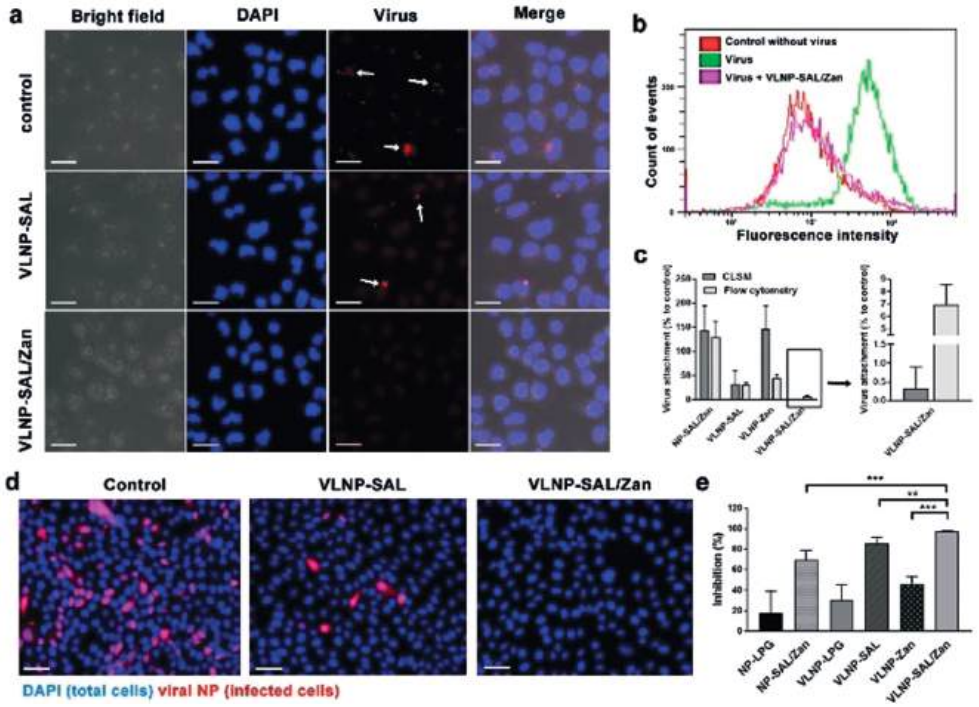

Figure 3. a) Projection CLSM images for virion binding to MDCK II cells in the presence of the inhibitors. Scale bar: 20 μm. b) Flow-cytometry analysis for the virion binding to MDCK II cells in the presence of VLNP-SAL/Zan. c) Virus attachment analysis for the CLSM images and flow-cytometry results. Values are expressed as mean ± SD, $n = 4$. d) Immunofluorescence staining of the viral NP to show the cellular infections at an MOI of 1. Scale bar: 50 μm, MOI = multiplicity of infection. e) Inhibition ratios for the nano-inhibitors from the counting of infected cells. Values are expressed as mean ± SD, $n = 4$. $^{**}p < 0.01$, $^{***}p < 0.001$ by Student t-test. Detailed data for other inhibitors are shown Figure S7 and S8.

nano-inhibitors with SAL functionalization. For VLNP-SAL/Zan, there was nearly no signal for virus being detected by CLSM, and the fluorescence intensity profile for the cells was identical to the no-virus control sample as shown in flow-cytometry, which confirms our hypothesis that the spiky nano-inhibitors can block virus binding to the host cells effectively.

With the proof of decoy binding, we then investigated whether the nano-inhibitors could inhibit influenza virus infection at the entry step. Immunofluorescence staining of viral NP in the infected cells was carried out. All cells were marked with the DAPI stain (blue) while the infected cells were additionally marked by staining of the viral NP (pink) as shown in Figure 3 d,e. In control cultures, 42.2 ± 6.6 % of the cells expressed viral antigen. Pre-treatment with the nano-inhibitors clearly reduced infection. Without SAL or Zan, there was no significant inhibition of viral infection, which excludes an effect by underivatized LPG for the viral inhibition (Figure S7). For the cells treated with VLNP-SAL and VLNP-Zan, the infection rates were 6.2 ± 2.8 % and 22.5 ± 2.9 %, respectively. Few to no infected cells (0.1 ± 0.1 %) were detected upon treatment with VLNP-SAL/Zan, which corresponds to an inhibition ratio higher than 99.9 %.

A potent influenza inhibitor should show robust inhibitory activity even when used after the infection. We evaluated inhibition of post-infection viral replication by the nano-inhibitors by using a multicyclic viral replication assay. In this assay, MDCK II cells were infected with virus at a multiplicity of infection (MOI) of 0.01, and then cultured in the medium supplied with the nano-inhibitors for 24 hours. Afterwards, the active virus in the medium was titrated by plaque assay to investigate viral replication. We first investigated the inhibitory effects on influenza A/X31 (H3N2) for the inhibitors at different concentrations from 50 to 1000 μg mL^{-1} (Figure 4 a). Potent inhibition with a reduction in viral titre of six orders of magnitude, corresponding to 99.9999 % inhibition, was achieved by VLNP-SAL/Zan at the cellular non-toxic dose, which support a therapeutic window for the inhibitor. With only 50 μg mL^{-1} VLNP-SAL, a reduction of 5 orders of magnitudes was achieved. NP-SAL/Zan showed potent inhibition at high doses, but at 50 μg mL^{-1}, the viral titre was reduced by only 2.5 orders of magnitudes, thus supporting the idea that the spiky nanostructures can enhance viral binding and inhibition. Similar inhibitory effects were obtained for infection with two other typical human IAV strains, A/PR/8/34 (H1N1) and A/Panama/2007/1999 (H3N2), which indicated that the VLNP-SAL/Zan might be broadly active in human IAV strains (Figure 4 b).

We also evaluated inhibition of viral replication at a late stage of infection with high viral load (Figure S9). In this case, the nano-inhibitors were used 24 hours post infection. Compared with the experimental settings for Figure 4 a,b, there were 2.5-fold more replication cycles, with approximately 10^8 PFU mL^{-1} virions in the medium before using the inhibitors. Reduction in viral titres was also achieved with VLNP-SAL/Zan, for which a reduction of 5 orders of magnitudes was achieved, which was slightly lower but in the same level as its performance in the early-stage inhibition. However, in this case, VLNP-SAL only showed a moderate inhibition of viral replication, with a reduction of just 2 orders of magnitudes.

The potent inhibitory effects indicate that the viruses might be neutralized by the nano-inhibitors in the medium. For verification, plaque-reduction assays were carried out (Figure 4 c–e). Dose-dependent plaque reduction (PR) curves were obtained by varying the nano-inhibitor concentrations (Figure 4 d) and the IC_{50} values were then estimated (Figure 4 e). VLNP-SAL/Zan showed the best plaque reduction performance, for which the $IC_{50(PR)}$ is 1.33 ± 0.14 μg mL^{-1}. The tendencies for VLNP-SAL and NP-SAL/Zan were similar to

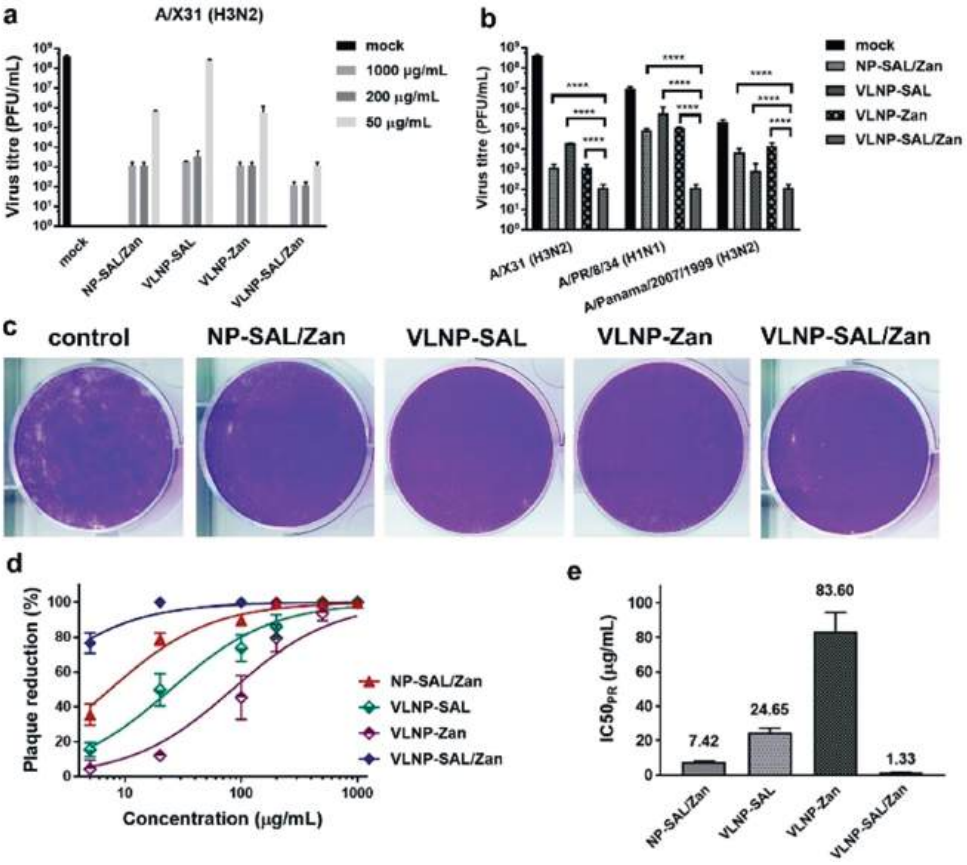

Figure 4. a) Inhibition of influenza A/X31 (H3N2) replication in the presence of the nano-inhibitors. b) Inhibition of virus replication at an inhibitor dosage of 1000 μg mL^{-1}. The inhibitors were introduced into the cell culture medium 45 min after the first cycle of viral infection. c) Representative images for the reduction of plaque formation of influenza A/X31 (H3N2) for inhibitors at a concentration of 100 μg mL^{-1}. d) Plaque-reduction ratios for the inhibitors at different concentrations. e) $IC_{50(PR)}$ values for the inhibitors towards influenza A/X31 (H3N2) from the plaque-reduction ratios. Values are expressed as mean ± SD, $n = 4$. ****$p < 0.0001$ by Student t-test.

that for VLNP-SAL/Zan, but with higher $IC_{50(PR)}$ values. For VLNP-Zan, only a slight reduction in viral activity was noticed. This also indicates efficient neutralizing of the virus, for which heteromultivalent engagement with both HA and NA is essential.

In conclusion, in this study, we demonstrated the topology-matching design of an IAV inhibitor that has a matching surface topology towards the IAV particle and shows dual inhibitory effects towards the two key proteins for viral binding. The synthesized nano-inhibitor is able to neutralize IAV virions extracellularly and block their binding to the host cells. As a result, robust inhibition (> 99.9999 % or a reductions of 6 orders of magnitude) of viral replication is achieved. We also envision that the idea of topology-matching design could be extended to the inhibition of other viruses, especially ones with a spiky morphology such as coronaviruses.

Acknowledgements

The authors gratefully acknowledge financial support from Deutsche Forschungsgemeinschaft (DFG) through grants within the Collaborative Research Center (SFB) 765. C.N. acknowledges the support from China Scholarship Council (CSC). We would like to acknowledge the assistance of the Core Facility BioSupraMol supported by the DFG. Open access funding enabled and organized by Projekt DEAL.

Conflict of interest

The authors declare no conflict of interest.

Keywords: antiviral agents · inhibitors · influenza · nanoparticles · topology matching

[1] a) D. Gatherer, *J. Clin. Virol.* **2009**, *45*, 174–178; b) G. J. D. Smith, D. Vijaykrishna, J. Bahl, S. J. Lycett, M. Worobey, O. G. Pybus, S. K. Ma, C. L. Cheung, J. Raghwani, S. Bhatt, J. S. M. Peiris, Y. Guan, A. Rambaut, *Nature* **2009**, *459*, 1122–1125; c) V. N. Petrova, C. A. Russell, *Nat. Rev. Microbiol.* **2018**, *16*, 47–60.

[2] a) M. Kanekiyo, M. G. Joyce, R. A. Gillespie, J. R. Gallagher, S. F. Andrews, H. M. Yassine, A. K. Wheatley, B. E. Fisher, D. R. Ambrozak, A. Creanga, K. Leung, E. S. Yang, S. Boyoglu-Barnum, I. S. Georgiev, Y. Tsybovsky, M. S. Prabhakaran, H. Andersen, W.-P. Kong, U. Baxa, K. L. Zephir, J. E. Ledgerwood, R. A. Koup, P. D. Kwong, A. K. Harris, A. B. McDermott, J. R. Mascola, B. S. Graham, *Nat. Immunol.* **2019**, *20*, 362–372; b) J. Wang, P. Li, Y. Yu, Y. Fu, H. Jiang, M. Lu, Z. Sun, S. Jiang, L. Lu, M. X. Wu, *Science* **2020**, *367*, eaau0810; c) C. I. Paules, S. G. Sullivan, K. Subbarao, A. S. Fauci, *N. Engl. J. Med.* **2018**, *378*, 7–9.

[3] a) R. E. Amaro, P. U. Ieong, G. Huber, A. Dommer, A. C. Steven, R. M. Bush, J. D. Durrant, L. W. Votapka, *ACS Cent. Sci.* **2018**, *4*, 1570–1577; b) H.-L. Yen, C.-H. Liang, C.-Y. Wu, H. L. Forrest, A. Ferguson, K.-T. Choy, J. Jones, D. D.-Y. Wong, P. P.-H. Cheung, C.-H. Hsu, O. T. Li, K. M. Yuen, R. W. Y. Chan, L. L. M. Poon, M. C. W. Chan, J. M. Nicholls, S. Krauss, C.-H. Wong, Y. Guan, R. G. Webster, R. J. Webby, M. Peiris, *Proc. Natl. Acad. Sci. USA* **2011**, *108*, 14264–14269.

[4] F. Krammer, *Nat. Rev. Immunol.* **2019**, *19*, 383–397.

[5] a) M. D. Vahey, D. A. Fletcher, *eLife* **2019**, *8*, e43764; b) P. H. Hamming, N. J. Overeem, J. Huskens, *Chem. Sci.* **2020**, *11*, 27–36; c) R. Wagner, T. Wolff, A. Herwig, S. Pleschka, H.-D. Klenk, *J. Virol.* **2000**, *74*, 6316–6323.

[6] a) S.-J. Kwon, D. H. Na, J. H. Kwak, M. Douaisi, F. Zhang, E. J. Park, J.-H. Park, H. Youn, C.-S. Song, R. S. Kane, J. S. Dordick,

K. B. Lee, R. J. Linhardt, *Nat. Nanotechnol.* **2017**, *12*, 48 – 54; b) S. Tang, W. B. Puryear, B. M. Seifried, X. Dong, J. A. Runstadler, K. Ribbeck, B. D. Olsen, *ACS Macro Lett.* **2016**, *5*, 413 – 418; c) S. Bhatia, D. Lauster, M. Bardua, K. Ludwig, S. Angioletti-Uberti, N. Popp, U. Hoffmann, F. Paulus, M. Budt, M. Stadtmüller, T. Wolff, A. Hamann, C. Böttcher, A. Herrmann, R. Haag, *Biomaterials* **2017**, *138*, 22 – 34; d) D. Lauster, M. Glanz, M. Bardua, K. Ludwig, M. Hellmund, U. Hoffmann, A. Hamann, C. Böttcher, R. Haag, C. P. R. Hackenberger, A. Herrmann, *Angew. Chem. Int. Ed.* **2017**, *56*, 5931 – 5936; *Angew. Chem.* **2017**, *129*, 6025 – 6030; e) M. A. Sparks, K. W. Williams, G. M. Whitesides, *J. Med. Chem.* **1993**, *36*, 778 – 783; f) D. Lauster, S. Klenk, K. Ludwig, S. Nojoumi, S. Behren, L. Adam, M. Stadtmüller, S. Saenger, S. Zimmler, K. Hönzke, L. Yao, U. Hoffmann, M. Bardua, A. Hamann, M. Witzenrath, L. E. Sander, T. Wolff, A. C. Hocke, S. Hippenstiel, S. De Carlo, J. Neudecker, K. Osterrieder, N. Budisa, R. R. Netz, C. Böttcher, S. Liese, A. Herrmann, C. P. R. Hackenberger, *Nat. Nanotechnol.* **2020**, *15*, 373.

[7] a) A. Harris, G. Cardone, D. C. Winkler, J. B. Heymann, M. Brecher, J. M. White, A. C. Steven, *Proc. Natl. Acad. Sci. USA* **2006**, *103*, 19123 – 19127; b) L. J. Calder, P. B. Rosenthal, *Nat. Struct. Mol. Biol.* **2016**, *23*, 853 – 858.

[8] a) P. Dey, T. Bergmann, J. L. Cuellar-Camacho, S. Ehrmann, M. S. Chowdhury, M. Zhang, I. Dahmani, R. Haag, W. Azab, *ACS Nano* **2018**, *12*, 6429 – 6442; b) M. W. Kulka, I. S. Donskyi, N. Wurzler, D. Salz, Ö. Özcan, W. E. S. Unger, R. Haag, *ACS Appl. Bio Mater.* **2019**, *2*, 5749 – 5759.

[9] a) S. Bhatia, L. C. Camacho, R. Haag, *J. Am. Chem. Soc.* **2016**, *138*, 8654 – 8666; b) J. Vonnemann, S. Liese, C. Kuehne, K. Ludwig, J. Dernedde, C. Böttcher, R. R. Netz, R. Haag, *J. Am. Chem. Soc.* **2015**, *137*, 2572 – 2579.

[10] W. Wang, P. Wang, X. Tang, A. A. Elzatahry, S. Wang, D. Al-Dahyan, M. Zhao, C. Yao, C.-T. Hung, X. Zhu, T. Zhao, X. Li, F. Zhang, D. Zhao, *ACS Cent. Sci.* **2017**, *3*, 839 – 846.

[11] M. Imai, Y. Kawaoka, *Curr. Opin. Virol.* **2012**, *2*, 160 – 167.

[12] J.-J. Shie, J.-M. Fang, P.-T. Lai, W.-H. Wen, S.-Y. Wang, Y.-S. E. Cheng, K.-C. Tsai, A.-S. Yang, C.-H. Wong, *J. Am. Chem. Soc.* **2011**, *133*, 17959 – 17965.

[13] a) J. L. McAuley, B. P. Gilbertson, S. Trifkovic, L. E. Brown, J. L. McKimm-Breschkin, *Front. Microbiol.* **2019**, *10*, 39; b) F. Wen, X.-F. Wan, *Trends Microbiol.* **2019**, *27*, 477 – 479.

[14] M. Müller, D. Lauster, H. H. K. Wildenauer, A. Herrmann, S. Block, *Nano Lett.* **2019**, *19*, 1875 – 1882.

[15] J. Haldar, L. Álvarez de Cienfuegos, T. M. Tumpey, L. V. Gubareva, J. Chen, A. M. Klibanov, *Pharm Res.* **2010**, 27, 259-263.

Manuscript received: April 2, 2020
Accepted manuscript online: May 18, 2020
Version of record online: July 8, 2020

